Origin of the Breit-Wigner-Fano lineshape of the tangential *G*-band feature of metallic carbon nanotubes

S. D. M. Brown, A. Jorio, and P. Corio
Department of Physics, Massachusetts Institute of Technology, Cambridge, Massachusetts 02139-4307

M. S. Dresselhaus
*Department of Physics and Department of Electrical Engineering and Computer Science, Massachusetts Institute of Technology,
Cambridge, Massachusetts 02139-4307*

G. Dresselhaus
Francis Bitter Magnet Laboratories, Massachusetts Institute of Technology, Cambridge, Massachusetts 02139-4307

R. Saito
Department of Electronics-Engineering, University of Electro-Communications, Tokyo 182-8585, Japan

K. Kneipp
*Technical University of Berlin, 10623 Berlin, Germany
and G. R. Harrison Spectroscopy Laboratory, Massachusetts Institute of Technology, Cambridge, Massachusetts 02139-4307*

A detailed line-shape analysis of the tangential *G*-band feature attributable to metallic single-walled carbon nanotubes is presented. Only two components are needed to account for the entire *G*-band feature for metallic nanotubes. The higher-frequency component has a Lorentzian line shape, and the lower one has a Breit-Wigner-Fano (BWF) line shape. Through comparisons of the Raman tangential *G*-band spectra from three different diameter distributions of carbon nanotubes, we find that both the frequency and linewidth of the BWF component are diameter dependent and show functional forms consistent with theory. The nanotube curvature is responsible for both the frequency differences between the two components of the characteristic metallic *G*-band spectrum and the BWF coupling of the lower-frequency component. Surface-enhanced Raman spectroscopy studies provide supporting evidence that the phonon BWF coupling is to an electronic continuum.

PACS number(s): 61.48.+c, 78.30.Na

I. INTRODUCTION

One method for distinguishing between *metallic* and *semiconducting* single-walled carbon nanotubes (SWNTs) in any given sample[1,2] is based on the distinct differences in the line shape of the tangential *G*-band (~ 1600 cm^{-1}) feature in their Raman spectra. The *G*-band of semiconducting nanotubes has been extensively studied, and is well accounted for using Lorentzian oscillators to describe the six Raman-active modes,[1,2] recently identified by polarization studies of the symmetries of the various line-shape components.[3] Some researchers previously fitted the Raman line shape for metallic SWNTs using Lorentzians[4,5] while others used a Breit-Wigner-Fano[6,7] (BWF) line shape to fit the lower-frequency component of the *G*-band spectrum. There has, however, been no explanation of the mechanism responsible for the downshift and broadening of the tangential *G* band of metallic SWNTs relative to semiconducting SWNTs.

The analysis presented here confirms that only two Raman components are needed to fit the tangential *G* band for metallic SWNTs,[7] with a Lorentzian line shape describing the higher-frequency feature and a BWF line describing the lower-frequency feature. Both components are found to exhibit predominantly *A* (A_{1g}) symmetry. The differences in their peak frequencies are attributed to (1) a difference in force constant for vibrations along the tube axis (higher force constant) versus circumferentially (lower force constant); and (2) an additional downshifting and broadening of the lower-frequency peak due to coupling of the discrete phonons to an electronic continuum, resulting in the BWF line shape.

The asymmetric BWF line shape,[8] described by

$$I(\omega) = I_0 \frac{[1 + (\omega - \omega_{\mathrm{BWF}})/q\Gamma]^2}{1 + [(\omega - \omega_{\mathrm{BWF}})/\Gamma]^2} \qquad (1)$$

(where $1/q$ is a measure of the interaction of the phonon with a continuum of states, and ω_{BWF} is the BWF peak frequency at maximum intensity I_0), has previously been used to fit some of the Raman bands of the metallic forms of various sp^2 carbons, such as the ~ 1540 cm^{-1} feature of metallic SWNTs,[6,7] the tangential *G*-band feature of alkali-metal doped SWNTs,[9] the feature near 1600 cm^{-1} of carbon aerogels[10] and alkali-metal graphite intercalation compounds,[11] as well as the ~ 270 cm^{-1} feature[12] of metallic K_3C_{60}. In contrast, the Raman bands of the *semiconducting* forms of sp^2 carbons [undoped C_{60} and K_6C_{60},[12] and semiconducting SWNTs (Ref. 3)] exhibit *Lorentzian* line shapes.

The inset to Fig. 1 shows the Stokes Raman signal (from 900 to 2000 cm^{-1}) from a sample of SWNTs with diameters $d_t = 1.49 \pm 0.20$ nm, for laser excitation energies $E_{\mathrm{laser}} = 1.58$ and 2.41 eV. The lower-frequency tail of the broad
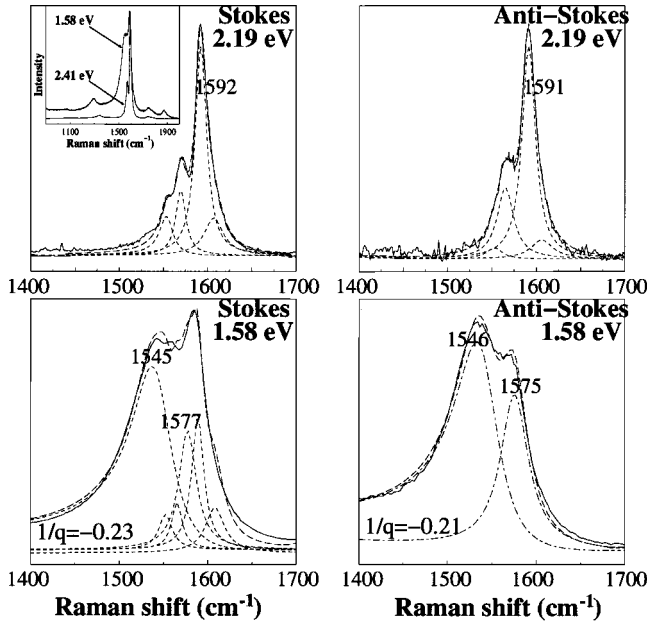
FIG. 1. Illustrative Stokes and anti-Stokes Raman spectra for the SWNT sample S1 with $d_t = 1.49 \pm 0.2$ nm taken at $E_{laser} = 1.58$ and 2.19 eV. Fitting parameters are listed in Table I. The inset presents Raman spectra in the spectral range from 900 to 2000 cm^{-1} showing results obtained from the same sample S1 using the laser excitation energies: 2.41 eV (lower curve) and 1.58 eV (upper curve).

tangential G band, obtained using $E_{laser} = 1.58$ eV excitation, comes from metallic SWNTs and exhibits a slow decay back to the spectral baseline (suggesting use of an asymmetric BWF line-shape analysis). This is in contrast to the flat baseline from $E_{laser} = 2.41$ eV in the inset to Fig. 1, for which the spectrum is associated with semiconducting SWNTs, and Lorentzian line shapes describe the spectra well.

In this paper we focus on the line-shape analysis of the tangential G-band feature in both the Stokes and anti-Stokes resonant Raman spectra for metallic SWNTs with different diameter distributions and different E_{laser} values. We here emphasize the coupling associated with the BWF line shape, compare theoretical predictions of the BWF parameters with experiment, describe the important role of SWNT curvature in the coupling process and, by analyzing the effect of surface-enhanced resonant Raman spectroscopy (SERRS) on the Raman bands of SWNTs, we gain insight into the electron-phonon coupling mechanism responsible for the BWF line shape in metallic SWNTs.

II. EXPERIMENT

Three different diameter distributions of SWNTs were used in this study, all synthesized through the arc discharge method using different synthesis conditions. Carbolex Inc. used a 4:1 ratio of a Ni:Y catalyst mixture to produce SWNTs with $d_t = 1.49 \pm 0.20$ nm (sample S1). The second sample (S2) used a 2.6 at. % Ni, 0.7 at. % Fe and 0.7 at. % Co catalyst mixture along with 0.75 at. % FeS, resulting in SWNTs with a broad distribution of diameters (mean diameter of $d_0 = 1.85$ nm).[13] The third sample (S3) was produced

TABLE I. Detailed line-shape analysis of the Stokes and anti-Stokes spectra from both metallic and semiconducting SWNTs with $d_t = 1.49 \pm 0.2$ nm, shown in Fig. 1 for $E_{laser} = 1.58$ and 2.19 eV. The frequencies (ω) and FWHM (Γ) are listed for the Lorentzian features, while additionally the $(1/q)$ value is given for the BWF features. The fitting parameters were obtained from the smallest root-mean-square error of the fitting procedure.

ω (cm^{-1}) 1.58 eV	Γ (cm^{-1}) (Stokes)	$1/q$	ω (cm^{-1}) 2.19 eV	Γ (cm^{-1}) (Stokes)	$1/q$
1545 [a]	56	−0.23			
1552 [b]	18		1553 [b]	19	
1565 [b]	14		1569 [b]	14	
1577 [a]	24				
1590 [b]	17		1592 [b]	15	
1608 [b]	26		1607 [b]	26	
1.58 eV	(anti-Stokes)		2.19 eV	(anti-Stokes)	
1546 [a]	61	−0.21			
			1553 [b]	22	
			1565 [b]	23	
1575 [a]	38				
			1591 [b]	18	
			1606 [b]	30	

[a]Metallic nanotubes.
[b]Semiconducting nanotubes.

using a 1 at. % Ni and 1 at. % Fe catalyst mixture, resulting in $d_t = 1.35 \pm 0.20$ nm. Surface-enhanced Raman scattering (SERS) experiments[14] were performed on sample S3 under resonance Raman scattering conditions (SERRS), where the Raman signal of the adsorbed nanotubes was strongly enhanced when the SWNTs were in contact with clusters of silver colloidal particles.[15–17]

The Raman experiments were performed under ambient conditions, using a backscattering configuration. For laser excitation radiation, we used the 514.5-nm (2.41 eV) line from an Ar$^+$ laser; the 632.8-nm (1.96 eV) line from an air-cooled He-Ne laser; the 568-nm (2.19 eV) line from a Kr$^+$ laser; the 782.0-nm (1.58 eV) line of a solid state Al-doped GaAs laser; and the 830-nm (1.49 eV) line of a Ti:sapphire laser.

III. RESULTS

Comparison fits to the tangential G-band features (obtained using $E_{laser} = 1.58$ and 2.19 eV) are shown in Fig. 1 for both the Stokes and anti-Stokes spectra taken from sample S1, using fitting parameters listed in Table I. Both the Stokes and anti-Stokes Raman spectra obtained for $E_{laser} = 2.19$ eV (where only semiconducting nanotubes are resonant in sample S1) show line shapes that are best fit by four Lorentzian oscillators[3] located at ∼1607, 1592, 1569, and 1553 cm^{-1}. These fits are based on polarization studies of the line shape,[3] with the anti-Stokes spectra requiring the
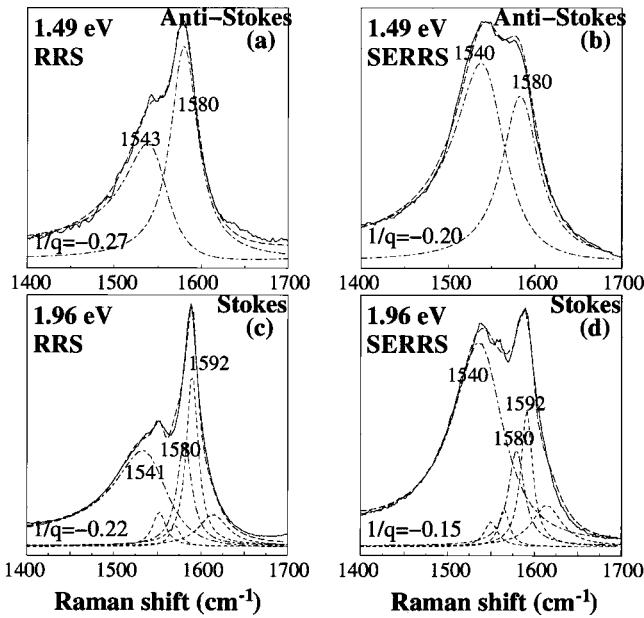
FIG. 2. Deconvolved spectra (taken on sample S3) of the anti-Stokes and Stokes tangential G-band obtained with $E_{laser}=1.49$ and 1.96 eV for normal resonant Raman spectroscopy (RRS) and for SERRS on silver surfaces. Fitting parameters for the Raman peaks associated with metallic nanotubes are listed in Table II.
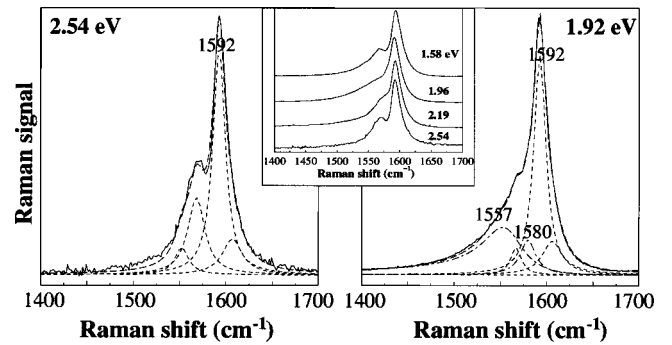

FIG. 3. Detailed line-shape analysis of the tangential G-band feature in the Stokes spectra from samples of nanotubes with a broad distribution of diameters centered at $d_0=1.85$ nm, collected using $E_{laser}=2.54$ and 1.92 eV. The inset shows the modest changes in the tangential G-band feature for this sample of SWNTs with changes in E_{laser}.

same oscillator frequencies but larger full width at half maximum (FWHM) linewidth values than the Stokes spectrum. A fit of these features to a BWF line shape yielded only very small $1/q$ values ($|1/q|<0.07$), showing that the same set of Lorentzian oscillators ($1/q\equiv0$) are sufficient to fit both the Stokes and anti-Stokes spectra for semiconducting SWNTs. We found this to be the case for the semiconducting nanotube Raman spectra for all three samples.

Figure 1 also shows both the Stokes and anti-Stokes Raman spectra from $E_{laser}=1.58$ eV. We chose this value of laser excitation energy since, for the *anti-Stokes* Raman spectrum, resonant contributions from only the metallic SWNTs of sample S1 ($d_t=1.49\pm0.20$ nm) contribute to the Raman tangential G-band feature.[18] The anti-Stokes spectrum is best fit using a BWF line shape for the 1546 cm^{-1} feature ($1/q=-0.21$) and a Lorentzian line for the 1575 cm^{-1} feature. In contrast, the *Stokes* spectrum of sample S1 from $E_{laser}=1.58$ eV, however, requires contributions from *both* metallic and semiconducting SWNTs, as explained in Ref. 18, to fit the entire tangential G-band spectrum (see Table I and Fig. 1). Fits to the tangential G band from sample S1 for other values of laser excitation energy, where metallic SWNTs are resonantly enhanced in the Stokes or anti-Stokes spectra (1.5 eV$<E_{laser}<2.1$ eV), similarly gave only two components for the Raman features of metallic nanotubes, with negative values of the $1/q$ interaction parameter ($0.14\leq|1/q|\leq0.26$) for the lower frequency BWF feature ($\omega_{BWF}=1544-1548$ cm^{-1}).

We also analyzed the tangential G-band feature for SWNTs with peak diameters smaller (sample S3) and larger (sample S2) than those of sample S1. Figure 2(a) shows the anti-Stokes tangential G-band feature for sample S3 (d_t

$=1.35\pm0.20$ nm), collected using $E_{laser}=1.49$ eV. This choice of laser excitation energy also allowed us to collect the tangential G-band feature from only metallic SWNTs from this sample ($d_0=1.35$ nm), since semiconducting nanotubes in sample S3 are not resonant at this E_{laser} value. The tangential G-band feature for sample S3 was also best fit using only two components, with a Lorentzian line shape at 1580 cm^{-1}, while the BWF component was located at a *lower* value of Raman shift (1543 cm^{-1}) than was found for sample S1, with $1/q=-0.27$. Fits to the tangential G band for this sample (S3) for other E_{laser} values yielded a frequency range for the BWF component (1539–1543 cm^{-1}), with $1/q$ values in the range $0.18\leq|1/q|\leq0.27$. The line shape of the Stokes tangential G band of sample S2 ($d_0=1.85$ nm) for $E_{laser}=2.54$ eV is typical of semiconducting SWNTs, and only modest changes of the tangential G-band feature were observed with decreasing E_{laser} (see the inset to Fig. 3). As resonance with metallic nanotubes is established upon lowering E_{laser} below 2.54 eV, a small BWF peak near 1557 cm^{-1} develops, with $1/q$ ranging from -0.12 to -0.25 (FWHM $\simeq40$ cm^{-1}). This contribution from metallic nanotubes to the Raman spectra for sample S2 is present in the tangential G-band feature down to $E_{laser}=1.58$ eV (see Fig. 3). However, for these large diameter nanotubes, no clearly resolved metallic components develop, as was the case for samples S1 and S3. Additionally, Kataura *et al.*[6] showed Raman spectra from SWNTs with 0.68 nm$\leq d_t$ ≤1.0 nm, and the lower-frequency (BWF) component was located at 1530 cm^{-1} ($1/q=-0.25$).

We also present the results of the SERRS (surface-enhanced *resonance* Raman spectroscopy) experiments performed on SWNT sample S3, where the sample was adsorbed on silver colloidal clusters,[15] and where there is an electronic resonance process operative along with the SERRS process. Figures 2(a) and 2(b), respectively, show the resonant Raman spectroscopy (RRS) and SERRS anti-Stokes G-band spectra ($E_{laser}=1.49$ eV) collected from sample S3. Both of these anti-Stokes G-band spectra were fit with similar (metallic) line shapes, although the SERRS features are broader and $1/q$ is decreased slightly relative to the

corresponding RRS features. However, the integrated intensity ratio $I^{\text{BWF}}_{1540}/I^{\text{Lor}}_{1580}$ is much larger for SERRS (2.21) than for RRS (0.75). A much smaller enhancement of the 1580 cm^{-1} feature by the chemical SERRS effect is seen by normalizing the fits of the I^{Lor}_{1580} peak at $E_{\text{laser}} = 1.96$ eV to I^{Lor}_{1592} for the corresponding 1592 cm^{-1} Lorentzian oscillator for sample S3 [see Figs. 2(c) and 2(d)], where the intensity ratio $I^{\text{Lor}}_{1580}/I^{\text{Lor}}_{1592}$ is seen to increase only slightly from 0.9 (RRS) to 1.1 (SERRS), but the same normalization gives a much larger intensity change for the 1540 cm^{-1} BWF feature, with $I^{\text{BWF}}_{1540}/I^{\text{Lor}}_{1592}$ increasing from RRS (3.5) to SERRS (7.2).

IV. DISCUSSION

Group theory predicts that there are six Raman-active modes within the tangential G-band spectral region (~ 1600 cm^{-1}) for general chiral SWNTs [two each of modes with A (A_{1g}), E_1 (E_{1g}), and E_2 (E_{2g}) symmetry].[3,19–21] The symmetry assignments of the four Lorentzian features (1553, 1569, 1592, and 1607 cm^{-1}) used to fit the semiconducting nanotube G-band feature also have been reported.[3] The Lorentzian components located at 1553 and 1607 cm^{-1} have been assigned to mode vibrations with E_2 (E_{2g}) symmetry,[3] with the contributions to the observed intensity coming mostly from small and high chiral angle SWNTs, respectively.[3,20,21] [We note that $\theta = 0°$ corresponds to zigzag (smallest chiral angle nanotubes), and $\theta = 30°$ to armchair (largest chiral angle nanotubes).] The feature at 1592 cm^{-1} has been assigned to unresolved A (A_{1g}) and E_1 (E_{1g}) symmetry mode vibrations from low chiral angle tubes, while the 1569 cm^{-1} feature is attributed to A (A_{1g}) and E_1 (E_{1g}) modes from high chiral angle tubes. The two E_1 and E_2 modes come from zone folding of the phonon dispersion bands *away* from the Γ point,[20–22] and so they are expected to have different frequencies. The two A modes are associated with the Γ point, and are therefore not expected to show any zone-folding splitting. However, the curvature of the nanotubes results in lower force constants for vibrations of the atoms in the circumferential direction as compared to vibrations along the nanotube axis, and this results in the two different frequencies of the A modes observed for the semiconducting nanotubes (1569 and 1592 cm^{-1}).[3] Furthermore, polarized Raman experiments have also shown that it is the two A (A_{1g}) components that are dominant in the intensity of the G-band Raman spectra from semiconducting SWNTs.[3]

Calculations also show that the displacements of the eigenvectors of the G-band phonons are always either parallel (LO) or perpendicular (TO) to the nanotube axis for the two phonon modes for each irreducible representation, and this symmetry effect does not depend on chiral angle θ.[20,21] Due to the directions of the atom displacements relative to the nanotubes axis after zone folding, Saito *et al.* have shown that zone folding of the LO vibrations of 2D graphite results in TO vibrations of the one-dimensional (1D) SWNTs (and vice versa) for the E_1 and E_2 modes.[20] (In this work, when we use the notation LO and TO, we are referring to modes for the 1D SWNTs.) As will be seen later, this results in the TO phonons for the 1D SWNTs having higher frequency than the LO phonons for the modes with E_1 (E_{1g}) and E_2 (E_{2g}) symmetry. As mentioned above, zone folding does not affect the modes with A symmetry, since they are at the Γ point. However, the curvature effect causes the A^{LO} mode (displacements along the SWNT axis) to have a higher frequency than the A^{TO} mode (displacements perpendicular to the SWNT axis) due to the reduction in the force constants because of the tube curvature. Saito *et al.* calculated the frequencies of the six modes comprising the tangential G-band region for a general chiral SWNT, and they are ordered, from lowest to highest frequency, to be $E^{\text{LO}}_2 < E^{\text{LO}}_1 < A^{\text{TO}} < E^{\text{TO}}_1 < A^{\text{LO}} < E^{\text{TO}}_2$.[20] Thus the component of the tangential G-band Raman spectra for semiconducting SWNTs has been very well explained. However, in this paper we show that additional considerations must be given to explain the tangential G-band Raman spectra for metallic SWNTs.

The six modes (E^{LO}_2, E^{LO}_1, A^{TO}, E^{TO}_1, A^{LO}, E^{TO}_2) are also expected to appear in the Raman spectra for general chiral metallic SWNTs. However, fits to the anti-Stokes Raman spectra from samples S1 and S2 (where only the Raman tangential G band for metallic SWNTs are present) indicate that we need only two components to account for the G-band feature (~ 1540 and ~ 1580 cm^{-1}). The ''antenna'' effect, where there is preferential absorption and emission of light polarized parallel to the tube axis (taken to be the Z direction), is expected to be strong for metallic SWNTs.[17,23,24] Duesberg *el al.*[17] confirmed the dominance of this antenna effect for metallic SWNTs, since, for polarized Raman measurements on a single bundle of SWNTs, they found that the Raman signal from the tangential G-band feature, attributed to metallic SWNTs, disappeared when the incident and scattered light were polarized perpendicular to the tube axis.[17,24] Similar results have been obtained for a fiber of partially aligned SWNTs.[25] Due to this antenna effect, modes with E_1 (E_{1g}) symmetry will be suppressed in the Raman spectra, since they can only be observed under cross-polarization of either the incident or scattered light (XZ or ZX configurations).[3] Similarly, the antenna effect will result in the suppression of modes with E_2 (E_{2g}) symmetry, since they are only observed for both incident *and* scattered light polarized perpendicular to the tube axis (XX configuration).[3] Modes of A (A_{1g}) symmetry (observed for the ZZ polarization) are expected to dominate the Raman spectra for metallic nanotubes. Furthermore, totally symmetric modes experience the greatest amount of enhancement in a RRS process through a Franck-Condon mechanism,[26] further confirming that the two components of the tangential G band for a general metallic chiral nanotube are most likely of A symmetry. Experimentally, we have observed only two components in the fits to the Raman spectra for metallic carbon nanotubes, and so we attribute these two components to the A^{TO} and A^{LO} modes from the chiral metallic nanotubes.

We now examine more closely the behavior of the two components of the tangential G band of the Raman spectra for the metallic SWNTs. The higher-frequency component of the G band is seen to show only a weak dependence on the SWNT diameter, as evidenced by its appearance at about the
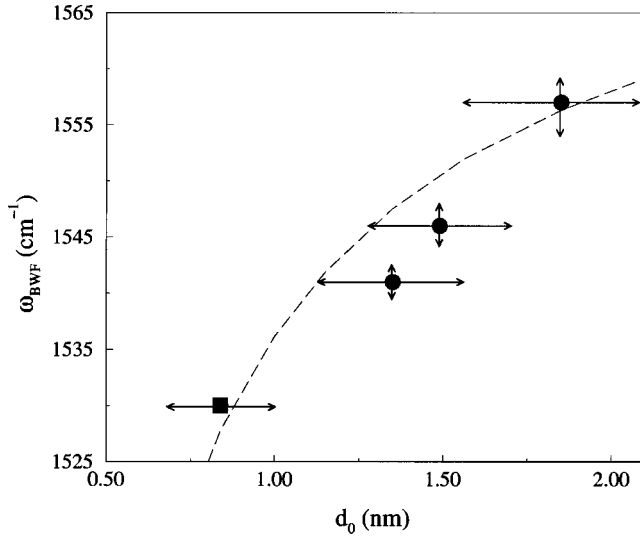
FIG. 4. The BWF peak frequency vs the mean nanotube diameter (d_0), where error bars reflect both the spread in the BWF peak frequency obtained from fits to the G band from different E_{laser} excitations, and the diameter distribution of the carbon nanotube samples. The points are located at d_0, the center of the diameter distribution. The square data point is taken from the literature (Ref. 6). The data points are fit using the functional form $\omega_{BWF} = \omega_0 + \alpha/d_t$, with values of the fitting parameters $\omega_0 = 1580$ cm^{-1} and $\alpha = -44$ cm^{-1} nm.

TABLE II. Fitting parameters (obtained from the smallest root-mean-square error of the fitting procedure) for only the Raman peaks of *metallic* SWNTs (dot-dashed curves) shown in Fig. 2 in the anti-Stokes ($E_{laser} = 1.49$ eV) and Stokes ($E_{laser} = 1.96$ eV) spectra collected from SWNTs ($d_t = 1.35 \pm 0.2$ nm) for normal RRS and SERRS (SWNTs adsorbed on silver surfaces).

| | $E_{laser} = 1.49$ eV | | | | | |
| RRS (anti-Stokes) | | | SERRS (anti-Stokes) | | |
ω (cm^{-1})	Γ (cm^{-1})	$1/q$	ω (cm^{-1})	Γ (cm^{-1})	$1/q$
1543	60	-0.27	1540	70	-0.20
1580	38		1580	52	

| | $E_{laser} = 1.96$ eV | | | | | |
| RRS (Stokes) | | | SERRS (Stokes) | | |
ω (cm^{-1})	Γ (cm^{-1})	$1/q$	ω (cm^{-1})	Γ (cm^{-1})	$1/q$
1541	72	-0.22	1540	76	-0.15
1580	11		1580	13	

same frequency (~ 1580 cm^{-1}) as in graphite and by its Lorentzian line shape in the fits to the three different diameter distributions of SWNTs (see Figs. 1, 2, and 3). The lower-frequency BWF component, on the other hand, shifts monotonically to lower frequencies as the diameter of the SWNTs gets smaller (see Fig. 4). For the large diameter SWNTs ($d_0 = 1.85$ nm) of sample S2, the frequency separation between the two components of the metallic G-band feature is $\Delta \simeq 1580 - 1557$ cm$^{-1} = 23$ cm^{-1}. This value of Δ is the same as the frequency separation between the two middle components of the semiconducting line shape ($\Delta \simeq 1592 - 1569$ cm$^{-1} = 23$ cm^{-1}).[3] For smaller diameter SWNTs, on the other hand, the frequency separation between the two components of the metallic G-band feature is much larger, increasing from $\Delta \simeq 23$ cm^{-1} for sample S2 (with $d_0 = 1.85$ nm) to $\Delta = 50$ cm^{-1} for SWNTs with $d_0 = 0.84$ nm (taken from Ref. 6). The curvature effect is operative for the semiconducting SWNTs as well, but in that case the frequency separation of the two middle components of the G band remains near ~ 20 cm^{-1} for the small diameter SWNTs. The much greater diameter dependence of Δ obtained for the metallic SWNTs cannot, therefore, be due solely to the difference in force constants for displacements along the nanotube axis in comparison to displacements in the circumferential direction.[3,20,21] We therefore turn to the influence of this BWF coupling on the resultant Raman feature in order to explain this greater frequency difference between the two A symmetry modes for metallic nanotubes.

Since metallic and semiconducting SWNTs have similar multiphonon continua, we can rule out the phonon continuum as the source of the BWF coupling. We then turn to

the electronic structure as the source of the continuum for the coupling mechanism. Since surface-enhanced Raman scattering (SERS) provides a means for perturbing the electronic structure of SWNTs, we consider this technique to provide insight into possible coupling mechanisms. We now turn to previously reported SERRS experiments[15,16] on sample S3, which are refit here using a BWF analysis (see Fig. 2 and Table II). Even though the intensity of the tangential G band from semiconducting SWNTs is enhanced by 10–12 orders of magnitude[15] in the SERRS experiment, the relative intensities of the Lorentzian oscillators in a fit to the G band of semiconducting tubes remain the same for the SERRS process relative to normal resonant Raman scattering (RRS).[16] However, for metallic SWNTs, not only is the intensity of the tangential G band enhanced, but the integrated intensity ratio $I_{1540}^{BWF}/I_{1580}^{Lor}$ (of the BWF component to the Lorentzian component) is also changed due to the chemical SERRS effect.[16] The chemical mechanism of SERRS enhancement can be described as a resonant Raman effect involving electronic levels of the SWNTs as modified by the adsorption of nanotubes onto the metal particles of the substrate.[14,16] Totally symmetric phonon modes are most sensitively affected by both the RRS process and by the chemical SERRS effect,[14] and thus the behavior of the two components of the Raman G-band spectrum for metallic SWNTs is again consistent with A (A_{1g}) symmetry.[16] Because the SERRS process greatly increases the BWF line intensity, we conclude that the coupling mechanism responsible for the BWF line shape relates to phonons coupling to a continuum based on collective excitations of the electrons.

The electronic density of states of metallic SWNTs is constant at the Fermi level over a large energy range, and therefore we can neglect the contribution from the van Hove singularities in the electronic density of states for energies near E_F. We assume that the coupling term between the electronic continuum and the discrete phonon line is proportional to the density of electronic states at the Fermi level (in units of the number of states per eV per C atom), and there-
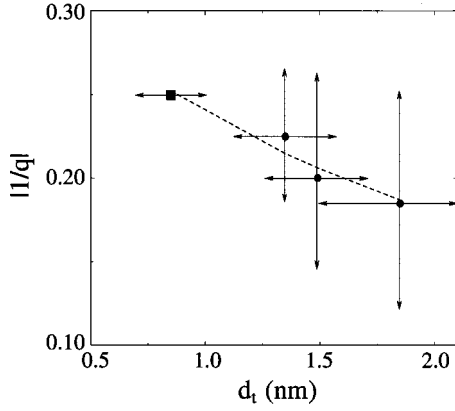
FIG. 5. The magnitude of the interaction parameter $(1/q)$ vs nanotube diameter (d_t). The data points are fit using the functional form $1/q = -1/(A \times d_t + B)$, with $A \sim 1.4$ nm^{-1} and $B \sim 2.8$.

FIG. 6. The FWHM linewidth (Γ) of the BWF peak plotted vs the Raman peak frequency found from fits to the Stokes tangential G-band feature (collected using different values of E_{laser}) associated with metallic nanotubes in samples S1 (circles), S2 (upward triangles), and S3 (downward triangles). The squares are data points taken from Ref. 6. The inset shows the FWHM linewidth vs mean nanotube diameter (d_0), where the error bars reflect contributions from both the FWHM linewidth and the nanotube diameter distribution.

fore inversely proportional to the tube diameter (d_t). The diameter dependence of the BWF peak frequency can be expressed as $\omega_{\text{BWF}} = \omega_0 + \alpha/d_t$, where ω_0 is the peak frequency in the absence of coupling to a continuum.[8] Figure 4 shows a plot of the peak frequency (ω_{BWF}) of the BWF component vs the mean diameter d_0 for the three SWNT samples studied in this work, along with a single data point (for small diameter SWNTs) taken from the literature (Ref. 6). Despite the various simplifications used in obtaining the theoretical expression, the data points are fairly well fit with the parameters set at $\omega_0 = 1580$ cm^{-1} and $\alpha = -44$ cm^{-1} nm. Thus the peak frequency of the BWF component (ω_{BWF}), in the fits to the tangential G-band feature, shifts to lower frequencies with decreasing diameter of the SWNTs, and converges to the G-band frequency of 1580 cm^{-1} at very large d_t. A more rigorous theoretical formulation will be necessary in the future to derive the functional form of ω_{BWF}, more accurately, taking the effect of nanotube curvature into account more completely.

The interaction parameter[8] $1/q$ is highly dependent on the baseline of each Raman spectrum, so that it is difficult to obtain reliable experimental information on $1/q$. However, $1/q$ is expected to take on the functional form

$$1/q = -1/(Ad_t + B), \qquad (2)$$

and the experimental data appear to show a tendency for the interaction parameter $(1/q)$ to have larger absolute values for smaller diameter SWNTs (see Fig. 5). From a fit to the above functional form, we obtain the values $A \sim 1.4$ nm^{-1} and $B \sim 2.8$ for the fitting parameters.

The FWHM linewidth (Γ) vs ω_{BWF} is plotted in Fig. 6, where we see that as the BWF peak shifts to lower frequencies, the feature broadens, consistent with a curvature-induced downshifting of the lower frequency A mode for these chiral metallic SWNTs, accompanied by a broadening due to BWF coupling. The inset to Fig. 6 shows that the BWF feature has a narrower linewidth (FWHM) for larger diameter SWNT samples. These results therefore indicate an
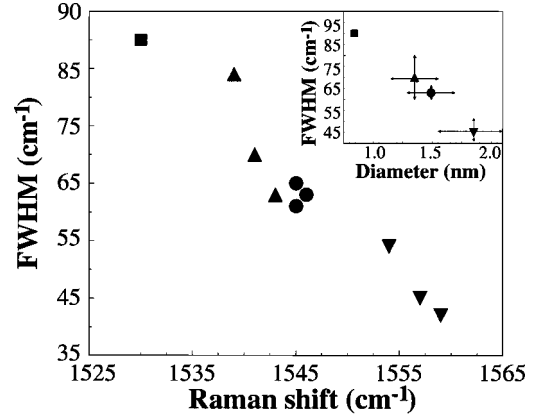
increased coupling of the discrete phonon line to a continuum, with the coupling increasing with decreasing diameter of the SWNTs.

It is apparent that the conduction electrons at the Fermi level play a crucial role in the appearance of the BWF coupled line shape for SWNTs, since only the metallic forms of curved carbon structures exhibit the BWF line shape. It is also very interesting to note that the peak frequency of the BWF feature appears at higher frequencies for the larger diameter SWNTs (see Fig. 4), which have lower curvature. Based on the negative sign of the $1/q$ coupling term in the BWF line shape,[11] we conclude from our RRS and SERRS experiments that the π-band conduction-electron plasmon is at an energy lower than $\hbar\omega_{\text{phonon}} = 0.19$ eV. The independently measured screened conduction electron plasma resonance frequency is $\hbar\omega_p = 0.15$ eV for multiwalled nanotubes,[27] and lies well below the G-band phonon for SWNTs.[28,29]

Saito *et al.* have reported that the A^{TO} phonon has a maximum Raman intensity for the polarization of light parallel to the nanotube axis,[30] thereby benefiting from the antenna effect. The TO phonon vibrations involve atom displacements in the circumferential direction, which would be sensitive to the nanotube diameter, and would account for the diameter dependence observed in the behavior of this lower-frequency component $[\omega_{\text{BWF}}(d_t)]$ of the metallic tangential G band. The curvature of the SWNTs would allow the coupling of these TO vibrations with the 1D π plasmons, resulting in the BWF line shape. The A^{LO} symmetry mode (the higher-frequency component) is expected to show little coupling to the electrons, since its displacements along the nanotube axis reproduces the situation in graphite (which shows no such BWF coupling), and thus it exhibits a Lorentzian oscillator line shape. We find experimentally that the BWF effect increases strongly with decreasing tube diameter (see, for ex-

ample, the inset to Fig. 6), which supports the plasmon continuum as the electron coupling mechanism, since smaller diameter nanotubes have larger curvature and hence stronger phonon-plasmon coupling.

The behavior of the Raman spectra of the metallic carbon nanotubes can also be compared to the behavior of graphite-alkali-metal intercalation compounds (GIC's), which show a BWF line shape for the lower stage forms. For high stage ($n \geq 3$) alkali-metal GIC's ($C_x M$ with $x \geq 36$), where M = K, Cs, or Rb, the high-frequency structure (~ 1600 cm^{-1}) is a doublet, both components of which are well fit with Lorentzian line shapes.[31] Ohana *et al.* showed that the BWF line shape which is observed for the high-frequency feature of the second-stage GIC C_{24}Rb was due to a discrete phonon line coupling to an electronic continuum.[32] For $E_{laser} = 1.83$ eV, the high-frequency feature of the second stage GIC developed an asymmetric (BWF) line shape (0.1 $\leq |1/q| \leq 0.4$), somewhat similar to the $1/q$ values for metallic SWNTs.[32] An extreme asymmetry (BWF line shape) was observed for the high-frequency feature in the Raman spectrum from first-stage ($C_8 M$, M = K, Cs, and Rb) alkali-metal GIC's, with much higher values of the $1/q$ interaction parameter ($0.3 \leq |1/q| \leq 1.3$) than is observed for metallic SWNTs.[11,31] The relatively large density of metallic donor atoms in GIC's results in a large increase in the carrier density in the conduction band, s electrons are transferred from the alkali-metal species to the graphene layers thereby giving rise to stronger plasmon effects in low stage GIC's. We also see that the peak position of the high-frequency BWF feature of the alkali-metal GIC's shifts to lower frequencies and that the FWHM linewidth (Γ) increases dramatically as the stage index decreases. We therefore see that for other sp^2 carbons an increased BWF coupling results in similar behavior to that observed and reported here for metallic SWNTs.

V. CONCLUSION

The differences between the tangential G-band Raman spectra from metallic and semiconducting SWNTs are discussed, with particular emphasis given to the characteristics of the BWF feature. A strong ''antenna'' effect is observed for the tangential G band of metallic SWNTs, which suppresses modes with E_1 (E_{1g}) and E_2 (E_{2g}) symmetry, thus effectively resulting in only modes with A (A_{1g}) symmetry appearing in the Raman spectra of metallic SWNTs. The curvature of the SWNTs accounts for the difference in frequency of the two A symmetry modes for semiconducting SWNTs. However, for metallic SWNTs, the curvature of the SWNTs facilitates increased BWF coupling of the lower-frequency metallic G-band component to a plasmon-based electronic continuum, which results in a greater downshifting and broadening of this feature as the tube diameter decreases. We were able to fit the BWF frequency (ω_{BWF}) fairly well using a functional form involving the electronic density of states at the Fermi level, and consistent results were obtained for fits to the experimental interaction parameter $1/q$ to theoretical predictions. The higher-frequency metallic G-band component (~ 1580 cm^{-1}), which has a Lorentzian line shape and exhibits a very weak dependence on the SWNT diameter, is attributed to the A^{LO} phonon which does not couple to the plasmon. The lower-frequency metallic G-band component is attributed to the A^{TO} phonon, which is expected to couple to the 1D π plasmon, and whose circumferential atom displacements are most sensitively affected by the curvature of the SWNTs. Experimental observations confirm these theoretical predictions qualitatively. Further work will be necessary to explain the curvature-dependent properties more quantitatively.

[1] A. M. Rao, E. Richter, S. Bandow, B. Chase, P. C. Eklund, K. W. Williams, M. Menon, K. R. Subbaswamy, A. Thess, R. E. Smalley, G. Dresselhaus, and M. S. Dresselhaus, Science **275**, 187 (1997).

[2] M. A. Pimenta, A. Marucci, S. D. M. Brown, M. J. Matthews, A. M. Rao, P. C. Eklund, R. E. Smalley, G. Dresselhaus, and M. S. Dresselhaus, J. Mater. Res. **13**, 2396 (1998).

[3] A. Jorio, G. Dresselhaus, M. S. Dresselhaus, M. Souza, M. S. S. Dantas, M. A. Pimenta, A. M. Rao, R. Saito, C. Liu, and H. M. Cheng, Phys. Rev. Lett. **85**, 2617 (2000).

[4] M. A. Pimenta, A. Marucci, S. Empedocles, M. Bawendi, E. B. Hanlon, A. M. Rao, P. C. Eklund, R. E. Smalley, G. Dresselhaus, and M. S. Dresselhaus, Phys. Rev. B **58**, R16016 (1998).

[5] S. L. Fang, A. M. Rao, P. C. Eklund, P. Nikolaev, A. G. Rinzler, and R. E. Smalley, J. Mater. Res. **13**, 2405 (1998).

[6] H. Kataura, Y. Kumazawa, Y. Maniwa, I. Umezu, S. Suzuki, Y. Ohtsuka, and Y. Achiba, Synth. Met. **103**, 2555 (1999).

[7] L. Alvarez, A. Righi, T. Guillard, S. Rols, E. Anglaret, D. Laplaze, and J.-L. Sauvajol, Chem. Phys. Lett. **316**, 186 (2000).

[8] M. V. Klein, in *Light Scattering in Solids I*, edited by M. Cardona (Springer-Verlag, Berlin, 1983), pp. 169–172.

[9] A. M. Rao, P. C. Eklund, S. Bandow, A. Thess, and R. E. Smalley, Nature (London) **388**, 257 (1997).

[10] G. A. M. Reynolds, A. W. P. Fung, Z. H. Wang, M. S. Dresselhaus, and R. W. Pekala, Phys. Rev. B **50**, 18 590 (1994).

[11] P. C. Eklund, G. Dresselhaus, M. S. Dresselhaus, and J. E. Fischer, Phys. Rev. B **16**, 3330 (1977).

[12] P. Zhou, K.-A. Wang, A. M. Rao, P. C. Eklund, G. Dresselhaus,

and M. S. Dresselhaus, Phys. Rev. B **45**, 10 838 (1992).

[13] C. Liu, H. T. Cong, F. Li, P. H. Tan, H. M. Cheng, K. Lu, and B. L. Zhou, Carbon **37**, 1865 (1999).

[14] A. Otto, I. Mrozek, H. Grabhorn, and W. Akemann, J. Phys.: Condens. Matter **4**, 1143 (1992).

[15] K. Kneipp, H. Kneipp, P. Corio, S. D. M. Brown, K. Shafer, J. Motz, L. T. Perelman, E. B. Hanlon, A. Marucci, G. Dresselhaus, and M. S. Dresselhaus, Phys. Rev. Lett. **84**, 3470 (2000).

[16] P. Corio, S. D. M. Brown, A. Marucci, M. A. Pimenta, K. Kneipp, G. Dresselhaus, and M. S. Dresselhaus, Phys. Rev. B **61**, 13 202 (2000).

[17] G. S. Duesberg, I. Loa, M. Burghard, K. Syassen, and S. Roth, Phys. Rev. Lett. **85**, 5436 (2000).

[18] S. D. M. Brown, P. Corio, A. Marucci, M. S. Dresselhaus, M. A. Pimenta, and K. Kneipp, Phys. Rev. B **61**, R5137 (2000).

[19] D. Kahn and J. P. Lu, Phys. Rev. B **60**, 6535 (1999).

[20] R. Saito, A. Jorio, J. Hafner, C. M. Lieber, M. Hunter, T. McClure, G. Dresselhaus, and M. S. Dresselhaus (unpublished).

[21] R. Saito, A. Jorio, G. Dresselhaus, and M. S. Dresselhaus, in The 25th International Conference on The Physics of Semiconductors, Osaka, edited by T. Ando (to be published).

[22] A. Kasuya, Y. Sasaki, Y. Saito, K. Tohji, and Y. Nishina, Phys. Rev. Lett. **78**, 4434 (1997).

[23] H. Ajiki and T. Ando, Physica B **201**, 349 (1994).

[24] C. Fantini, M. A. Pimenta, M. S. S. Dantas, D. Ugarte, A. M. Rao, A. Jorio, G. Dresselhaus, and M. S. Dresselhaus (unpublished).

[25] H. H. Gommans, J. W. Alldredge, H. Tashiro, J. Park, J. Magnuson, and A. G. Rinzler, J. Appl. Phys. **88**, 2509 (2000).

[26] R. J. H. Clark and T. J. Dines, Angew. Chem. **25**, 131 (1986).

[27] F. Bommeli, L. Degiorgi, P. Wachter, W. S. Bacsa, W. A. de Heer, and L. Forro, Solid State Commun. **99**, 513 (1996).

[28] A. M. Rao (private communication).

[29] A. Ugawa, A. G. Rinzler, and D. B. Tanner, Phys. Rev. B **60**, R11 305 (1999).

[30] R. Saito, T. Takeya, T. Kimura, G. Dresselhaus, and M. S. Dresselhaus, Phys. Rev. B **57**, 4145 (1998).

[31] S. A. Solin, Mater. Sci. Eng. **31**, 153 (1977).

[32] I. Ohana, M. S. Dresselhaus, and S. Tanuma, Phys. Rev. B **43**, 1773 (1991).